

## Flow characteristics of an air jet in a Mach 3 crossflow

A. O. Wills<sup>1</sup>, S. F. McCreton<sup>1</sup>, Z. Zhang<sup>1</sup>, M. Awasthi<sup>1</sup>, C. J. Doolan<sup>1</sup>, D. J. Moreau<sup>1</sup> and W. A. Miller<sup>2</sup>

<sup>1</sup>School of Mechanical and Manufacturing Engineering  
University of New South Wales, Sydney, 2052, Australia

<sup>2</sup>School of Mechanical Engineering  
University of Adelaide, Adelaide, 5005, Australia

### Abstract

The unsteady wake and wall pressures surrounding sonic injection into supersonic crossflow were investigated in experiments and LES simulations. The experiments and simulations were conducted in a Mach 3 flow with a 2 Bar sonic injector. Experimental wall-normal pressure profiles downstream of an jet inlet show lower pressures within the boundary layer region compared to the no-injection case, and an increase in pressure above that of the freestream values in the region passing through the jet plume. Mass flux spectra in the jet plume, and wall pressure spectra around the inlet show a significant broadband increase due to injection. The rise in wall pressure fluctuation intensity was greater closer to the jet, with the spectra returning to undisturbed levels much more gradually downstream of the inlet compared to upstream. Similar trends were also observed in the RMS wall pressure measurements.

### Introduction

The interaction of a sonic jet with a supersonic crossflow is a highly complex fluid dynamics problem present in air-breathing hypersonic aircraft, which generates a significant dynamic response on the structure [1]. The physics controlling the interaction, and the mean flow-field, have been the subject of a considerable body of work [4, 5], as a result the mean flow features surrounding the injection location are well understood. The time-averaged flow structures are shown in figure 1. The key features of the shock structure consists of a bow shock (4) and re-circulation region ahead of the jet (9), a Prandtl-Meyer expansion fan centred at the edge of the jet nozzle (8), barrel shock (3), and a Mach disk (5).

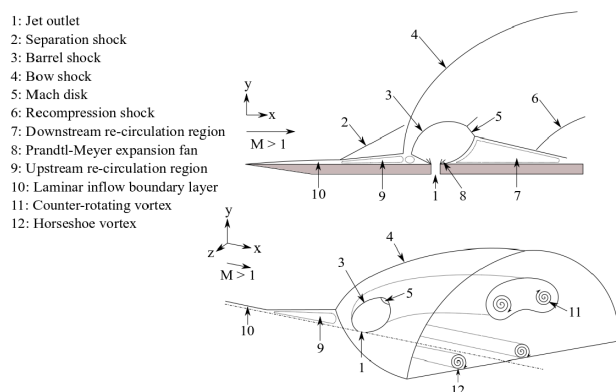


Figure 1: Schematic of the two- and three-dimensional interaction flow-field [6].

Conversely, the flow structures experience substantial temporal variations which are much less understood. The shock structure surrounding the inlet contains a number of unsteady features [8, 10] which are somewhat coupled [3]. Additionally many

vortices are shed from the interaction [11] which impart unsteady loads on the structure.

The present work aims to experimentally quantify the frequency response of the flow-field directly aft of the injection site as well as analyse the unsteady wall pressure around the injection. Wall-normal pitot pressure profiles will also be analysed downstream of the injection site.

### Experimental Setup

#### UNSW Mach 3 Wind Tunnel

Experimental measurements were performed in the UNSW supersonic wind tunnel (figure 2). This is a blow-down to atmosphere facility using compressed atmospheric air as the test gas, which is able to sustain Mach 3 flow for up to 20 seconds. The test section has a rectangular cross section measuring  $100 \times 142$  mm, and access is provided through a number of circular openings in the wall. Multiple smoothing screens are located upstream of the settling chamber to condition the flow prior to acceleration. The test section is followed by a parallel diffuser and exhaust system.

The temperature and pressure in the settling chamber both decrease over a single run, resulting in variation to the flow Reynolds number. This behaviour has been characterised and is highly repeatable. A typical pressure and Reynolds number per unit length profile for a single run is shown in figure 3.

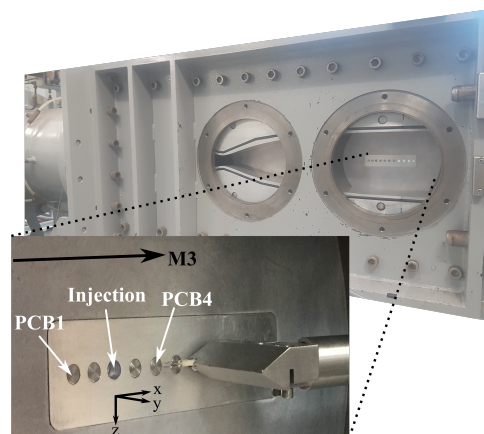


Figure 2: The UNSW supersonic wind tunnel and, insert, the measurement configuration for the current tests. Co-ordinate axis is shown, and the origin is set as the injection location.

#### Measurement Configuration

A specialised wall insert was 3D printed from ABS plastic capable of flush mounting multiple PCB 112A22 pressure transducers, as well as the gas injection port. All mounting ports are in the same streamwise location. When flush mounted, the

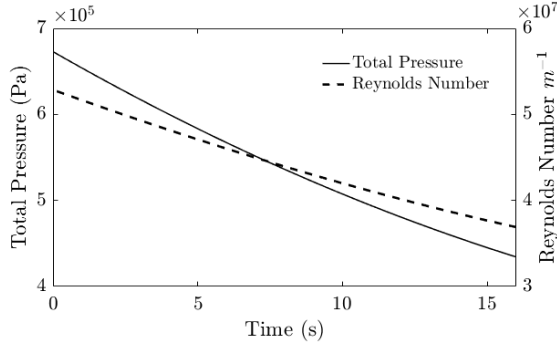


Figure 3: Typical pressure and Reynolds Number variation over a single run.

PCB sensors suffer from signal attenuation above 60kHz and appropriate corrections were applied to account for this [2]. The mounting locations in the wall inset had a spacing of  $2D$ , where  $D$  is the gas injection diameter, ranging from  $4D$  upstream to  $12D$  downstream of the jet. A custom made wedge shaped mount was used to support up to two hotwire or pitot probes simultaneously in the flow, and was capable of moving 20 mm through the boundary layer in the wall-normal direction. A boundary layer pitot probe was utilised for pressure measurements at  $y < 10$  mm due to limitations of the wedge mount, while straight probes were used for measurements further out from the wall. Both probes have an internal diameter of 1 mm. Pitot pressures were recorded using a 50 psi MKS Baratron pressure transducer.

Measurements of mean and fluctuating mass-flux were taken with a single-sensor hotwire probe with a  $5 \mu\text{m}$  diameter Platinum-plated Tungsten wire spot-welded between two metal prongs which were 1.25 mm apart. The hotwire probe was placed 15 mm from the wall and measurements were made with and without the gas injection. The response of a hotwire in supersonic flow is a function of both the mass-flux and the temperature fluctuations [7]. However, if the wire is operated at high overheat ratios then the hotwire responds only to the cooling due to mass-flux [9]. In the present work, the wire overheat ratio was set to 0.8. The standard hotwire calibration procedure [7] was performed by placing the hotwire in the free-stream and recording its voltage as a function of the varying mass-flux provided by the tunnel operation. The hotwire probe was connected to Dantec Dynamic multi-channel CTA 54N80 anemometer which measures the sensor wire resistance variation with flow speed through a wheatstone bridge and also consists of a servo amplifier to keep the bridge balanced. The CTA can also be used to regulate the sensor temperature by varying the amount of current passing through it.

The voltage output of all probes was acquired using National Instruments PXI 6124 DAQ modules, with terminal block attachments. Data was recorded at 500 kHz for the length of the run, with a one second window centred around a freestream total pressure of  $P_0 = 550$  kPa isolated for analysis.

Gas injection was controlled programatically via monitoring of the stagnation pressure to ensure the same flow conditions each run, while minimising the time of injection and amount of compressed gas used. The injected gas entered the test section with jet static pressure of  $P_j = 200$  kPa while sonic and The injection lasted for 3 seconds centred around  $P_0 = 550$  kPa.

#### Computational Setup

Simulations were performed using a pre-existing solver,

adapted to match the experimental flow conditions. The compressible, unsteady Navier–Stokes equations in dimensional form were solved using the rhoCentralFoam finite volume solver as part of the open-source OpenFOAM code [6]. An implicit Large Eddy Simulation (LES) methodology has been adopted to model turbulence. The mesh was structured with hexahedral cells concentrated in the region of the jet orifice as well as through the boundary layer. The mesh spacing was increased linearly in all directions from these concentrated regions; for a more detailed description of the mesh and solver setup see Ref [6].

The flow parameters for both the experiment and simulation are summarised in table 1. Here  $D$  is the jet diameter in mm,  $P$  is pressure in kPa, and subscripts  $j$  and  $\infty$  represent jet and freestream parameters respectively.  $J$  is the jet to crossflow momentum ratio defined as  $J = \rho_j U_j^2 / \rho_\infty U_\infty^2$ , where  $\rho$  is the density in  $\text{kg/m}^3$  and  $U$  is velocity in  $\text{m/s}$ .

	$M_\infty$	$M_j$	$D$	$P_j$	$P_j/P_\infty$	$J$
Experiment	3	1	5.5	200	13.3	1.9
Simulation	3	1	2	200	67	9.6

Table 1: flow parameters for both experiment and simulation.

Despite variation in flow parameters between the simulation and experiment, the simulation is still able to capture the physics of the interaction and provide global flow visualisation, something that is not possible from the current experimental setup. The information gleaned from the simulation aids in interpretation of the experimental results.

#### Results and Discussion

An LES time-averaged pressure gradient image of the flow-field is shown in figure 4. Key flow features shown in figure 1 are evident here, such as the upstream bow, barrel, and separation shocks, as well as the highly turbulent regions downstream of the injection.

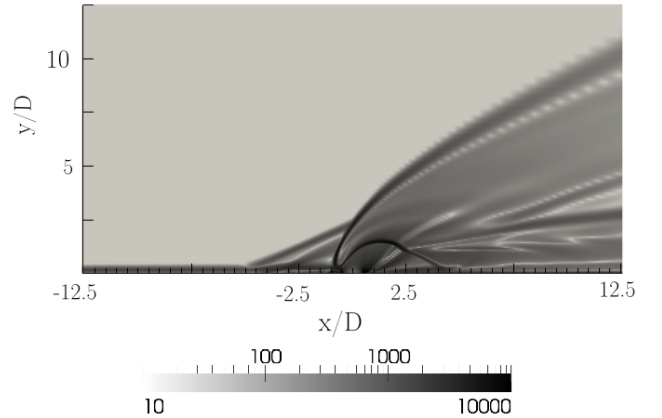


Figure 4: Time-averaged pressure gradient of the x-y plane along the centreline. Colourbar scale is  $\Delta p/\rho$ .

#### Total Pressure Profiles

Figure 5 shows wall-normal pitot pressure profiles measured with and without injection. Profiles were recorded  $4D$  downstream of the injection location on the centre line.

The pitot-pressure profile was first measured for the clean boundary layer case, and displays a typical boundary layer pro-

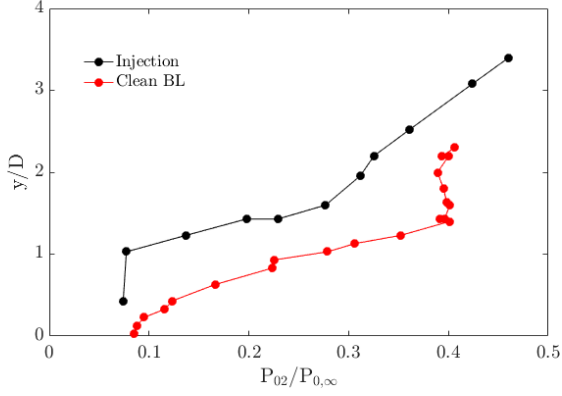


Figure 5: Experimental wall-normal pressure profiles for clean boundary layer (BL), and 4D downstream of the injection location on the centreline.  $P_{02}$  is the recorded pressure, and  $P_{\infty}$  is the freestream pressure.

file. The boundary layer height was found to be 6.5mm. Downstream of the injection site, the pitot profile matches the trend of the clean case up to a height of  $y/D=1.5$ , albeit with an offset. Beyond  $y/D=1.5$  the pitot probe enters the injection plume, and the profile begins to increase linearly.

#### Mass Flux

Mean and RMS mass flux profiles in the undisturbed boundary layer measured in the wall-normal direction using two hotwire probes are shown in figure 6. The mean profile shape agrees well with the pressure profile in figure 5. The RMS profile highlights the high level of turbulence within the boundary layer, compared to the minimal turbulence in the freestream.

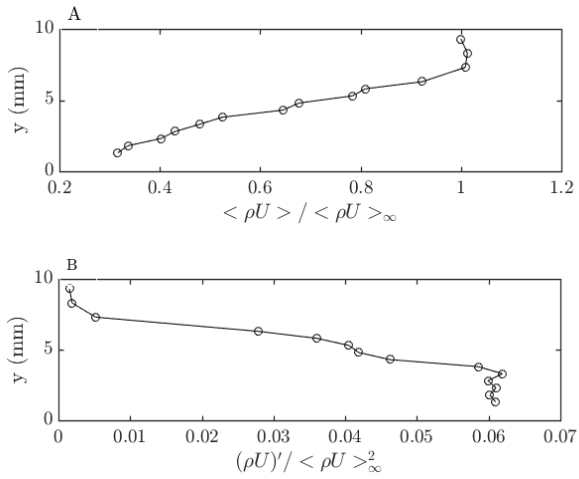


Figure 6: (a) Mean and (b) RMS of mass flux, in an undisturbed boundary layer.

An additional mass flux reading was taken at a wall normal distance of  $y/D=3$ , and 4D downstream of the jet inlet, for both undisturbed and injection cases. The mass-flux was calculated to be  $360 \text{ kg/m}^2\text{s}$  and  $400 \text{ kg/m}^2\text{s}$  without and with gas-injection respectively. The time series and mass-flux spectra for both cases are shown in figure 7. The inclusion of injection creates a broadband increase in the fluctuating mass flux over the entire measurable frequency range up to 20 kHz.

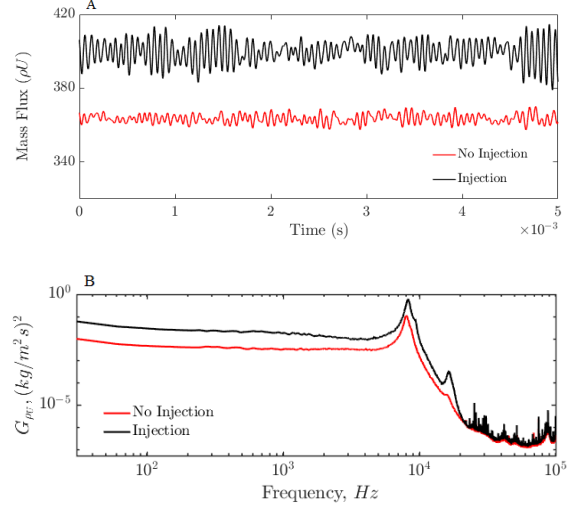


Figure 7: (a) Time series (b) Spectra of mass flux, for both injection and no injection cases.

#### Unsteady Wall Pressure Measurements

Wall pressure measurements were taken upstream and downstream of the injection location, along the centreline (figure 2 insert). The wall pressure was recorded at two locations upstream, and six downstream of the jet both with and without injection.

Figure 8 shows the RMS pressure measured at the wall in the streamwise direction. Without injection the RMS is effectively constant along the test section, as is expected for a zero pressure gradient boundary layer. It can be clearly seen that injection significantly impacts the RMS pressure in the vicinity of the injection site. A steep rise in RMS pressure is observed upstream of the jet, with the RMS pressure returning to a level similar to that of the clean boundary layer by 4 diameters upstream. The pressure rise downstream of the jet is significantly larger than upstream, and is accompanied by a much more gradual return to baseline level, requiring in excess of 12 diameters.

Both the up- and downstream pressure rises are related to the size of their respective recirculation regions which can be seen in figures 1 and 4. The turbulence and recirculation region downstream of the jet is significantly larger than its upstream counterpart, which causes a higher RMS pressure, and more gradual return to undisturbed levels.

Analysis of the wall pressure spectra provides a more detailed picture of the flow behaviour around the jet inlet. The spatial distribution of wall pressure spectra measured in the streamwise direction for the undisturbed boundary layer and jet-crossflow interaction are shown in figures 9 and 10 respectively. A white bar has been overlaid between  $-0.5D$  and  $+0.5D$  representing the location of the jet.

The clean boundary layer spectral map shows negligible variation in spectral content with position (figure 9), with a flat response up to the 100 kHz shown. The addition of a jet alters the frequency content of the wall pressure in this region. At all locations the spectra in figure 10 undergo a broadband increase compared to the clean boundary layer case, with larger energy levels closer to the injection site.

At 2D downstream of the jet the spectra display an increase of more than a decade in comparison to the spectra of the undisturbed boundary layer. This increase becomes less significant

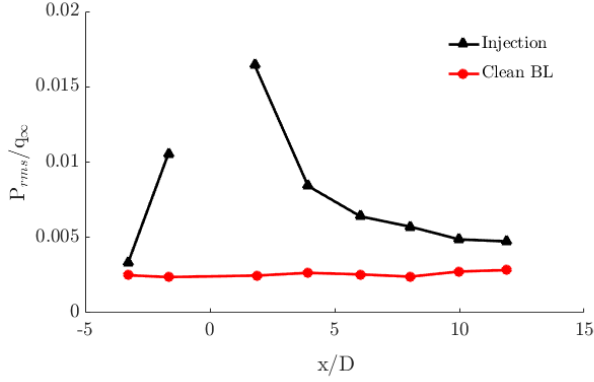


Figure 8: RMS of the wall pressure measured in the streamwise direction along the centreline.

as distance from the injector increased. At 12D downstream the spectra have returned to the undisturbed levels at frequencies below 10 kHz, with a broad hump occurring at 50kHz.

Upstream of the injection site, the fluctuations increase more quickly with a one decade growth in the frequency range below 10 kHz occurring within roughly 4D. Additionally, a much more gradual roll off is observed compared to the downstream spectra, beginning at 10 kHz.

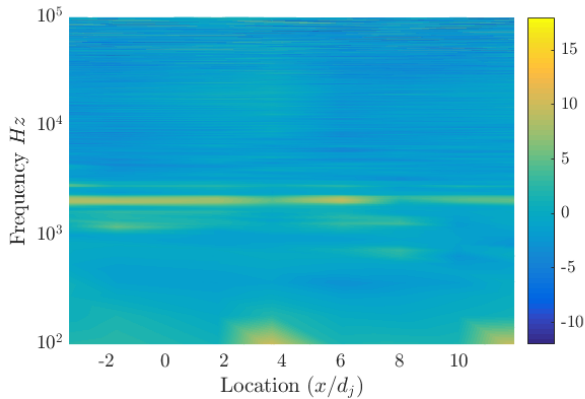


Figure 9: Spatial distribution of the wall pressure spectra under a clean boundary layer. Colourbar scale is  $10\log_{10}(Pa^2/Hz)$

## Conclusions

The unsteady flow-field surrounding a sonic, 2 Bar, jet in Mach 3 cross flow has been investigated. The unsteady wall pressure was measured both up and downstream of the jet along the centreline. Pressure profiles and mass flux reading were also taken downstream of the injection site. The injection caused a 10% increase in mean mass flux, as well as a broadband increase in the mass flux spectra when compared to the no-injection case.

The profiles showed the location of the jet plume downstream of the inlet, and the increase in pressure compared to the undisturbed boundary layer case. Mass flux readings were taken downstream of the injection site. The injection caused a 10% increase in mean mass flux, as well as a broadband increase in the mass flux spectra when compared to the no-injection case.

The unsteady wall pressures showed a broadband 1 decade increase in energy levels close to the injection site, decreasing as downstream the distance increased. Both the RMS pressures and frequency spectra highlighted the difference in size of the upstream and downstream recirculation regions, with the down-

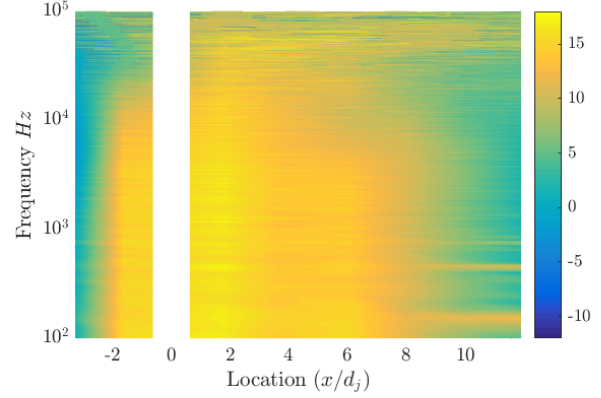


Figure 10: Spatial distribution of the wall pressure spectra around the injection location, white bar indicates the location and size of the ejector. Colourbar scale is  $10\log_{10}(Pa^2/Hz)$

stream region being over five times the length of the upstream region.

## References

- [1] Bolender, M. A. and Doman, D. B., Nonlinear longitudinal dynamical model of an air-breathing hypersonic vehicle, *Journal of Spacecraft and Rockets*, **44**, 2007, 374–387.
- [2] Corcos, G., Resolution of pressure in turbulence, *The Journal of the Acoustical Society of America*, **35**, 1963, 192–199.
- [3] Kawai, S. and Lele, S. K., Large-eddy simulation of jet mixing in supersonic crossflows, *AIAA journal*, **48**, 2010, 2063–2083.
- [4] Mahesh, K., The interaction of jets with crossflow, *Annual Review of Fluid Mechanics*, **45**, 2013, 379–407.
- [5] Margason, R., Years of jet in cross flow research. computational and experimental assessment of jets in crossflow, pages 1.1-1.41, 1993, Technical report, AGARD-CP-534, 50.
- [6] Miller, W. A., Medwell, P. R., Doolan, C. J. and Kim, M., Transient interaction between a reaction control jet and a hypersonic crossflow, *Physics of Fluids*, **30**, 2018, 046102.
- [7] Motallebi, F., A review of hot-wire technique in compressible flows, *NASA STI/Recon Technical Report N*, **94**.
- [8] Santiago, J. G. and Dutton, J. C., Velocity measurements of a jet injected into a supersonic crossflow, *Journal of Propulsion and Power*, **13**, 1997, 264–273.
- [9] Smith, D. R. and Smits, A. J., Simultaneous measurement of velocity and temperature fluctuations in the boundary layer of a supersonic flow, *Experimental Thermal and Fluid Science*, **7**, 1993, 221–229.
- [10] VanLerberghe, W. M., Santiago, J. G., Dutton, J. C. and Lucht, R. P., Mixing of a sonic transverse jet injected into a supersonic flow, *AIAA Journal*, **38**, 2000, 470–479.
- [11] Viti, V., Neel, R. and Schetz, J. A., Detailed flow physics of the supersonic jet interaction flow field, *Physics of Fluids*, **21**, 2009, 046101.